Journal of Industrial and Engineering Chemistry 80 (2019) 106–111

Contents lists available at ScienceDirect

Journal of Industrial and Engineering Chemistry

journal homepage: www.elsevier.com/locate/jiec

Transparent 3 nm-thick MoS_2 counter electrodes for bifacial dye-sensitized solar cells

Taehee Jeong[a,1], So-Yeon Ham[b,1], Bonkee Koo[a], Phillip Lee[c,*], Yo-Sep Min[b,*], Jae-Yup Kim[d,*], Min Jae Ko[a,*]

[a] Department of Chemical Engineering, Hanyang University, Seoul, 04763, Republic of Korea
[b] Department of Chemical Engineering, Konkuk University, Seoul, 05029, Republic of Korea
[c] Photo-Electronic Hybrids Research Center, Korea Institute of Science and Technology (KIST), Seoul 02792, Republic of Korea
[d] Department of Chemical Engineering, Dankook University, Yongin, 16890, Republic of Korea

ARTICLE INFO

Article history:
Received 6 June 2019
Received in revised form 10 July 2019
Accepted 20 July 2019
Available online 27 July 2019

Keywords:
Molybdenum disulfide
Atomic layer deposition
Bifacial solar cells
Counter electrode

ABSTRACT

Molybdenum disulfide (MoS_2) counter electrode (CE) is considered one of the most viable alternatives to Pt CE in dye-sensitized solar cells (DSSCs) owing to its abundance, low cost, and superior electrocatalytic activity. However, mostly, MoS_2 CEs for DSSCs are prepared by conventional chemical reactions and annealing at a high temperature. By these conventional processes, deposition of sufficiently thin and transparent MoS_2 layers is challenging; therefore, bifacial DSSCs employing transparent MoS_2 CEs have not been studied. Here, we report transparent few-nanometer-thick MoS_2 CEs prepared by atomic layer deposition at a relatively low temperature (98 °C) for bifacial DSSC applications. MoS_2 nanofilms with precisely controlled thicknesses of 3–16 nm are conformally coated on transparent conducting oxide glass substrates. With increase in the MoS_2 nanofilm thickness, the MoS_2 CE electrocatalytic activity for the iodide/triiodide redox couple enhances, but its transparency decreases. Notably, the application of a thinner MoS_2 nanofilm in a bifacial DSSC leads to lower conversion efficiency under front-illumination, but higher conversion efficiency under back-illumination. In particular, only the 3 nm-thick MoS_2 nanofilm shows reasonable photovoltaic performances under both front- and back-illumination conditions.

Introduction

Next-generation solar cells including organic solar cells [1,2], dye-sensitized solar cells (DSSCs) [3–8], quantum dot solar cells [9–11], and perovskite solar cells [12–15] have gained much attention as potential alternatives to the conventional crystalline Si solar cells because of their attractive properties such as low production cost, light weight, ease of fabrication, and potential flexibility. In particular, mesoscopic DSSCs have unique advantages over other emerging solar cells; they exhibit colorful and semitransparent features, high indoor performances, and reliable performances [4,16,17]. For these reasons, they are considered promising building-integrated photovoltaics (BIPVs), which utilize the incident light from both inside and outside of buildings [8,18–21].

For application in window-type BIPVs, DSSCs require transparent counter electrodes (CEs), which are suitable for bifacial operations. The conventional platinum (Pt) CE prepared by thermal decomposition or sputtering exhibits sufficient transparency for the bifacial DSSC application and excellent electrocatalytic activity for the iodide/triiodide redox couple. However, the low availability and high cost of Pt restrict the large-scale applications of DSSCs [4,22,23]; therefore, various types of Pt-free electrocatalysts have been investigated as CE materials, including metal sulfides [24–28], nitrides [22,29], and carbides [30]. In addition, carbon-based materials such as carbon nanotubes [31,32] and graphene [33,34], and conducting polymers [18,35] have been explored.

Among the Pt-free electrocatalysts, molybdenum disulfide (MoS_2) is considered one of the most viable alternatives to Pt owing to its abundance, low cost, superior electrocatalytic activity, and chemical stability [26–28,36–38]. In addition to the DSSC application, MoS_2 has been applied in various fields including electronics and catalysis because of its attractive properties

* Corresponding authors.
E-mail addresses: phillip@kist.re.kr (P. Lee), ysmin@konkuk.ac.kr (Y.-S. Min), jykim@dankook.ac.kr (J.-Y. Kim), mjko@hanyang.ac.kr (M.J. Ko).
[1] These authors contributed equally to this work.

https://doi.org/10.1016/j.jiec.2019.07.037
1226-086X/

stemming from the two-dimensional structure, such as high mobility, large specific surface area, as well as excellent catalytic activity [39–45]. Mostly, MoS_2 CEs for DSSCs have been prepared by conventional chemical reactions at 200–800 °C, followed by high-temperature annealing at 300–500 °C [26–28,36–38]. However, by these conventional processes, deposition of sufficiently thin MoS_2 layers is challenging; therefore, bifacial DSSCs employing transparent MoS_2 CEs have not been studied. In addition, the high-temperature annealing process is not suitable for plastic substrates used in flexible DSSCs. For the application of flexible plastic substrates, a low-temperature process lower than 150 °C is required [6].

Accordingly, we have developed few-nanometer-thick MoS_2 CEs by atomic layer deposition (ALD) for application in bifacial DSSCs (see the schematic illustration in Fig. 1). MoS_2 thin layers with precisely controlled thicknesses from 3 nm to 16 nm are conformally coated onto transparent conducting oxide glass substrates. Notably, this process is carried out at a relatively low temperature of 98 °C, which is suitable for flexible plastic substrates. DSSCs with 3 nm-thick MoS_2 CEs exhibit reasonable conversion efficiencies under both front- and back-illumination conditions. The electrocatalytic activities of the MoS_2 CEs and photovoltaic performances of the fabricated bifacial DSSCs are systemically investigated as a function of the MoS_2 layer thickness.

Experimental section

Preparation of MoS_2 and Pt CEs

Typically, a FTO glass substrate (Pilkington TEC-8) was cleaned in deionized water and ethyl alcohol under sonication for 15 min, separately, followed by drying with a stream of nitrogen gas. Then, the FTO glass surface was exposed to ultraviolet-ozone (UV/O_3) for 15 min at room temperature. For MoS_2 CE preparation, MoS_2 was deposited onto the UV/ozone-treated FTO glass substrate in a laminar-flow-type ALD reactor [45]. $Mo(CO)_6$ and dimethyldisulfide (DMDS, Aldrich) were used as the Mo and S sources, respectively. ALD was performed at 98 °C for a given number of cycles, each consisting of the following steps: $Mo(CO)_6$ exposure (4 s)–N_2 purging (30 s)–DMDS exposure (1.5 s)–N_2 purging (30 s). The film growth per cycle measured for MoS_2 deposited on a silicon wafer by spectroscopic ellipsometry was 0.11 nm per cycle. For comparison, conventional Pt CEs were prepared by the hydrothermal decomposition method. Typically, a drop of 7 mM H_2PtCl_6 solution in 2-propanol was spin coated on an FTO glass substrate, followed by annealing at 400 °C for 20 min in air [23,34].

Fabrication of DSSCs

To prepare the TiO_2 working electrode, firstly, a semitransparent paste including nanocrystal TiO_2 with 20 nm diameter was prepared by the procedure reported elsewhere [6,10]. In brief, TiO_2 nanoparticles were synthesized by a hydrothermal process and followed by mixing with lauric acid (Fluka) and ethyl cellulose (Aldrich) in α-terpineol (Fluka). The weight ratio of the components: TiO_2/lauric acid/ethyl cellulose/α-terpineol was 0.18:0.02:0.05:0.75. Before deposition of the prepared TiO_2 paste, a washed FTO glass substrate was treated with a blocking layer of dense TiO_2 by spin coating with a 7.0 wt% Titanium(IV) bis(ethylacetoacetato)-diisopropoxide solution in butyl alcohol and followed by heat treatment at 450 °C for 15 min in air. On the pretreated substrate, the semitransparent TiO_2 paste was coated by the doctor-blading technique and followed by annealing at 500 °C for 35 min in air. For the adsorption of sensitizers, the annealed TiO_2 film was dipped into 0.5 mM ethanol solution of N-719 dye (Everlight) for 15 h. Subsequently, the dye-sensitized working electrode was covered with the MoS_2 CE using 60 μm-thick hot-melt Surlyn (Dupont 1720). A drop of iodide/triiodide (I^-/I_3^-) electrolyte was injected into the assembled DSSCs through pre-drilled holes on the MoS_2 CE. The electrolyte was comprized of 0.03 M I_2 (Aldrich, 99.8%), 0.7 M 1-propyl-3-methylimidazolium iodide (PMII, synthesized in the lab), 0.5 M 4-tert-butylpyridine (Aldrich, 96%), and 0.05 M guanidinium thiocyanate (Aldrich, 97%) in acetonitrile. The active area of the cells was ~0.45 cm^2, as determined from the images obtained with a CCD camera (Moticam 1000), using an image analysis program.

Characterization

The absorption properties of the MoS_2 CEs were analyzed using UV–Vis spectroscopy (Agilent 8453). The surface electronic states of the MoS_2 CEs were examined by XPS (Thermo Fisher Scientific Sigma Probe) equipped with an Al K_α X-ray source (beam energy : 1486.6 eV). CV measurements were conducted on the MoS_2 CEs in an electrolyte comprising 1 mM I_2, 10 mM Li, and 0.1 M $LiClO_4$ in acetonitrile using a CHI440 potentiostat–galvanostat (CH Instruments Inc.). A Pt wire and the silver/silver ion (Ag/Ag^+) couple were utilized as the counter and reference electrodes, respectively; the scan rate was 50 mV/s. Standard J–V measurements were carried out using a solar simulator (Yamashita Denso YSS-200A) equipped with a 1600 W xenon lamp and an AM 1.5 G filter; the power was 100 mW/cm^2. For exact J–V measurements, an aperture mask was attached on each DSSC to prevent overestimation due to additional illumination through the lateral space [2,3]. The intensity of incident light was calibrated with a Si reference solar cell (National Renewable Energy

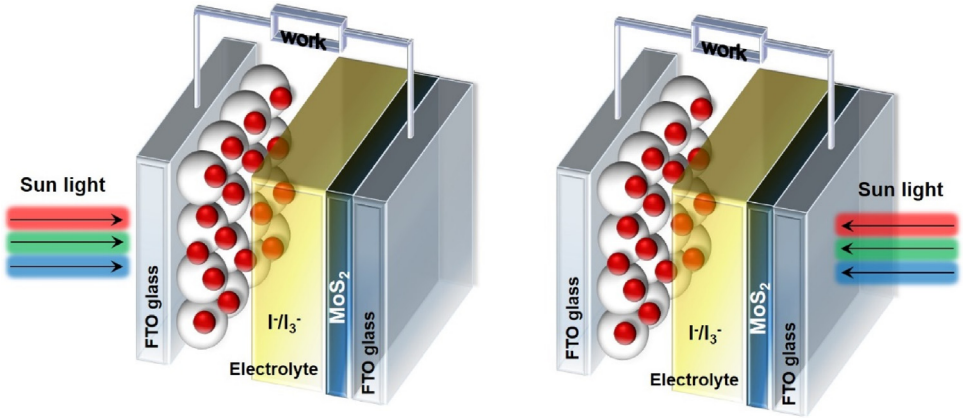

Fig. 1. Schematics of bifacial DSSC with MoS_2 CE under front- and back-illumination.

Laboratory). The incident IPCE spectra were obtained at short-circuit condition with a specially designed system using a 75 W xenon lamp source and a grating monochromator (PV Measurements Inc.). The spectral resolution was 10 nm. Symmetric dummy cells were fabricated by assembling two identical MoS_2 CEs with hot-melt Surlyn, followed by the injection of iodide/triiodide electrolyte. The impedance spectra and Tafel polarization curves of the dummy cells were obtained by using a Solartron 1287 potentiostat. The active area of the dummy cell was ~1.00 cm^2.

Results and discussion

Fig. 2 shows the digital photographs and specular transmittance spectra of MoS_2-deposited fluorine-doped tin oxide (FTO) glass samples as a function of the MoS_2 layer thickness (3, 9, and 16 nm; hereafter, referred to as MoS_2-3 nm, MoS_2-9 nm, and MoS_2-16 nm). Although the transmittance of MoS_2/FTO glass gradually reduces with increase in the MoS_2 layer thickness, all samples exhibit semitransparency in the entire visible-light region. The specular transmittances at 535 nm (N-719 absorption peak position) of bare FTO glass, MoS_2-3 nm, MoS_2-9 nm, and MoS_2-16 nm, are ~69.6, 63.0, 52.2, and 43.3%, respectively. In particular, MoS_2-3 nm shows a transmittance comparable to that of bare FTO glass. The difference in specular transmittance between bare FTO glass and MoS_2-3 nm is only 6.6% at 535 nm, and less than 8% in the entire visible range. These results imply that the MoS_2/FTO glass samples prepared by ALD have sufficiently high transparencies for bifacial solar cell applications.

X-ray photoelectron spectroscopy (XPS) was performed to examine the chemical states of the MoS_2 films prepared by ALD. The high-resolution XPS profile of MoS_2-16 nm in Fig. 3 shows Mo 3d and S 2p peaks. The peaks at 229.8 eV and 232.9 eV are assigned to the Mo(IV) $3d_{5/2}$ and Mo(IV) $3d_{3/2}$ states, respectively, and those at 162.4 eV and 163.7 eV are assigned to the S $2p_{3/2}$ and S $2p_{1/2}$ states, respectively. These data agree well with those reported for MoS_2 films [46]. Furthermore, the profile shows Mo(VI) $3d_{3/2}$ (236.6 eV) and Mo(VI) $3d_{5/2}$ (233.8 eV) peaks, implying that the film surface is partially oxidized because of exposure to air. Furthermore, in our previous study, X-ray diffraction analysis revealed that the as-prepared MoS_2 films prepared by ALD possessed amorphous phases [47].

The electrocatalytic activities of MoS_2 CEs for the iodide/triiodide redox couple were investigated by cyclic voltammetry (CV) as a function of the MoS_2 layer thickness (Fig. 4a). Two typical

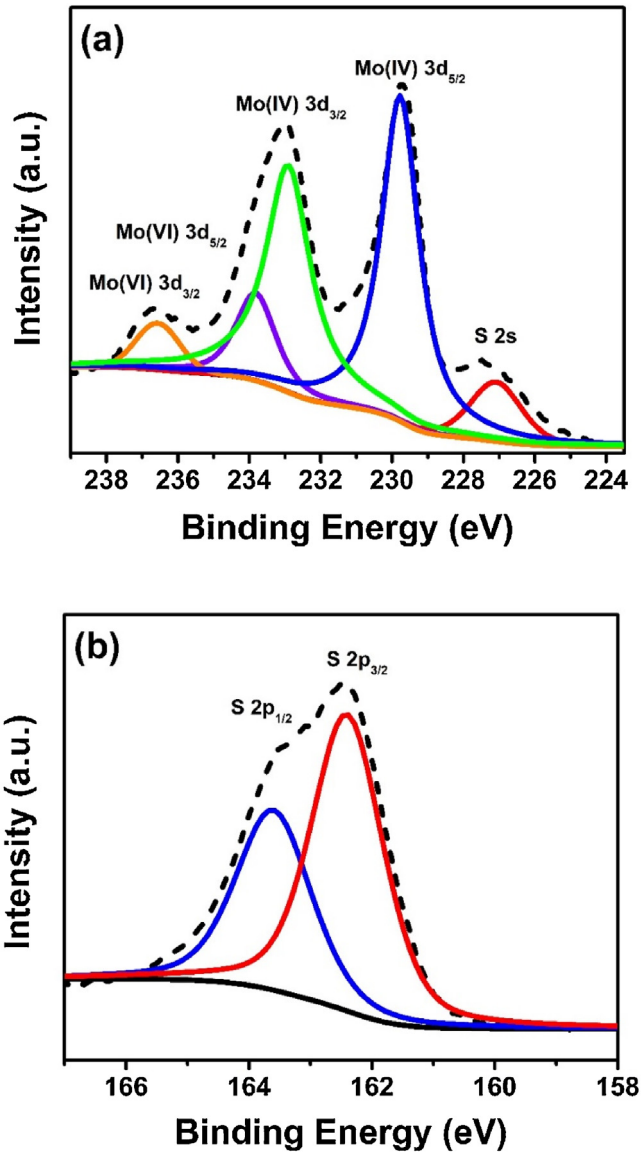

Fig. 3. (a) Mo 3d and (b) S 2p XPS profiles of MoS_2-16 nm.

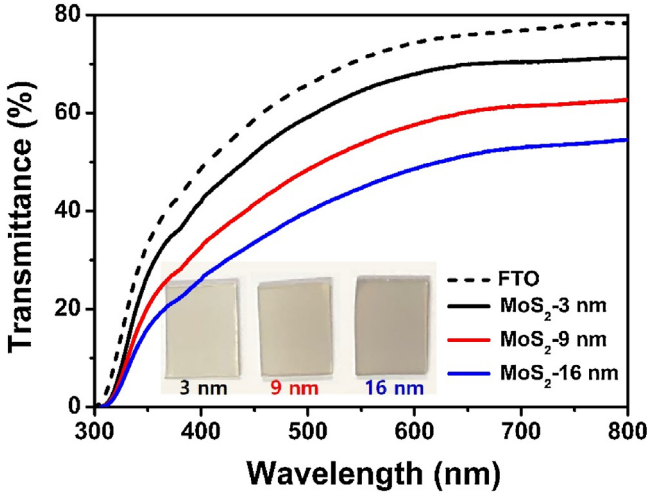

Fig. 2. Specular transmittance spectra of MoS_2/FTO glass samples, as a function of MoS_2 layer thickness. The images in the inset are digital photographs of MoS_2/FTO glass samples.

pairs of redox peaks were observed for all CEs, confirming the electrocatalytic activities of the prepared CEs for the iodide/triiodide redox couple. The more positive pair corresponds to the iodine/triiodide (I_2/I_3^-) redox reaction, and the more negative pair is assigned to the iodide/triiodide (I^-/I_3^-) redox reaction [6,22,26]. The redox current density gradually enhances as the thickness of the MoS_2 layer increases, implying that the thicker the film, the higher is the electrocatalytic activity.

The trend in electrocatalytic activity was cross-checked by Tafel polarization curves of symmetric dummy cells fabricated with the MoS_2 CEs, as shown in Fig. 4b. The exchange current density (J_0) was estimated from the intersection of the extrapolated linear branches in the limiting diffusion zone [23,34]. A steep slope of the Tafel curve implies high J_0 and high electrocatalytic activity for the iodide/triiodide redox couple. As shown in Fig. 4b, among the three cells, the one with the thickest MoS_2 film exhibits the highest J_0, which accords well with the CV data. Because ALD is considered an ideal method for conformal coating [48,49], the surface of the FTO glass substrate is expected to be fully covered with MoS_2, even in the case of MoS_2-3 nm. However, in our previous work, the thinner the MoS_2 nanofilm, the lower is its conductivity [45]. Therefore, the

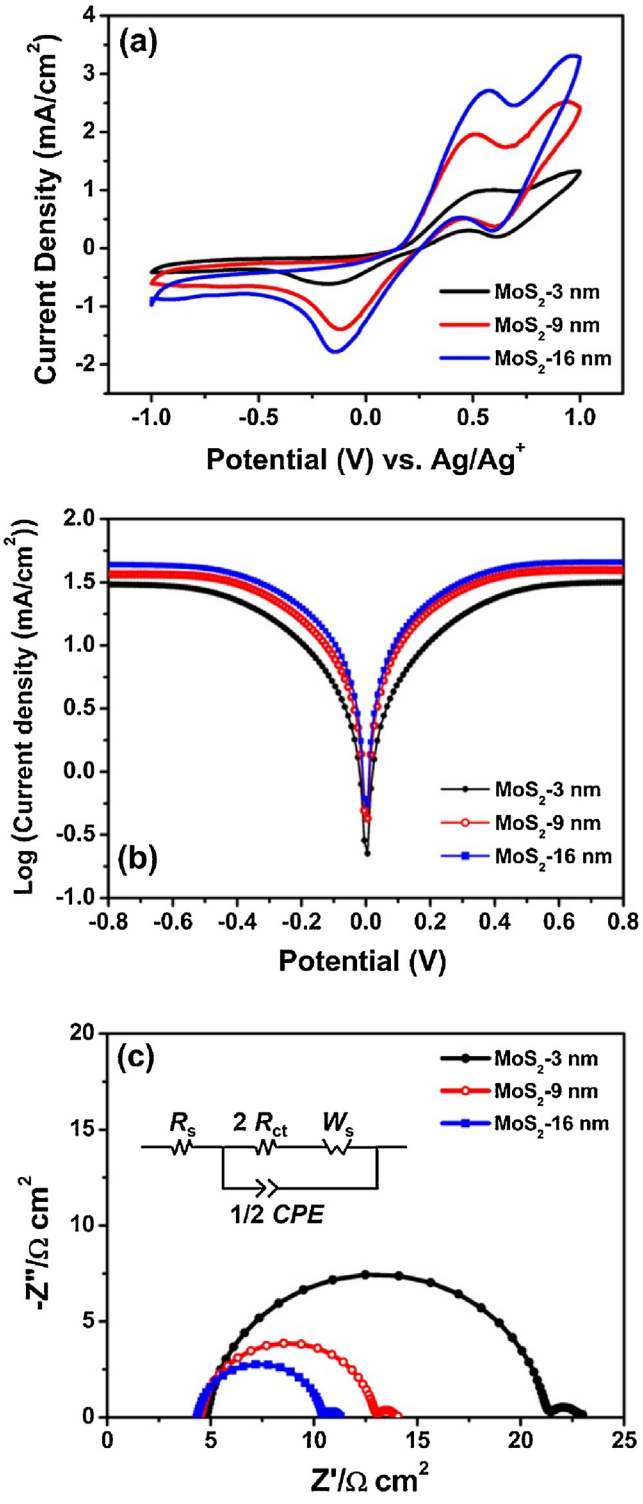

Fig. 4. (a) Cyclic voltammograms of MoS_2 CEs for the iodide/triiodide redox couple, as a function of MoS_2 layer thickness. (b) Tafel polarization curves and (b) impedance spectra (inset: equivalent circuit model) of symmetric dummy cells with MoS_2 CEs for the iodide/triiodide redox couple.

higher electrocatalytic activity of the 16 nm-thick MoS_2 film prepared in this study can be attributed to the more efficient charge transport through the deposited MoS_2 layer, compared to that in the other two samples.

For the quantitative comparison of the electrocatalytic activity depending on the thickness of MoS_2 layer, the impedance spectra of the symmetric dummy cells were obtained, as shown in Fig. 4c. The inset in Fig. 4c shows the corresponding equivalent circuit model comprising the series resistance (R_s), finite Warburg impedance (W_s), and impedance at the electrolyte/CE interface (R_{ct} and CPE). For electrodes with relatively rough surfaces, the CPE is generally used instead of a capacitor, and W_s is the impedance related to electrolyte diffusion [50,51]. Double-layer capacitance (C_{dl}) can be obtained from the CPE parameters. We fitted the impedance spectra using the ZView software, and evaluated the R_s, R_{ct} and C_{dl} values for all samples.

The R_s values, which is chiefly related to the sheet resistance of the electrodes [51–53], are 4.78, 4.51 and 4.35 Ω cm^2 for MoS_2-3, MoS_2-9, and MoS_2-16 nm, respectively. This slight decrease of R_s is attributed to the higher conductivity of the thicker MoS_2 film, as already mentioned before. The R_{ct} values for MoS_2-3, MoS_2-9, and MoS_2-16 nm are 8.41, 4.38, and 3.15 Ω cm^2, respectively, and the C_{dl} values are 2.10×10^{-5}, 2.20×10^{-5}, and 2.28×10^{-5} μF/cm^2, respectively. The trend in R_{ct} implies that the thicker the MoS_2 film, the higher is the electrocatalytic activity [22,34], which accords well with the CV data and Tafel polarization curves. As observed, C_{dl} does not considerably change with the film thickness, indicating that these samples have similar surface areas for electrochemical reaction [22,26,34]. This result is consistent with our assumption that the MoS_2 film entirely covers the surface of FTO glass, even in the case of MoS_2-3 nm. The CV curves, Tafel plots, and impedance data indicate that the thicker the MoS_2 film, the higher is the electrocatalytic activity for the iodide/triiodide redox couple.

The fabricated MoS_2 CEs were applied in bifacial DSSCs containing the iodide/triiodide electrolyte, and their photovoltaic properties were studied as a function of the MoS_2 layer thickness. Fig. 5a presents the photocurrent density–voltage (J–V) characteristics of DSSCs with MoS_2 films of different thicknesses under front-illumination. The photovoltaic performance parameters determined from the J–V curves are listed in Table 1. As the MoS_2 film thickness increases, the short-circuit current (J_{SC}) and open-circuit voltage (V_{OC}) slightly change, but the fill factor (FF) considerably increases, leading to a gradual enhancement of the conversion efficiency. MoS_2 films with thicknesses more than 16 nm could not be prepared because of experimental limitations.

Although the conversion efficiency gradually increases with increase in the MoS_2 film thickness, the DSSC with the 3 nm-thick film exhibits a reasonable efficiency of 5.52%, indicating the excellent electrocatalytic activity of MoS_2. The conversion efficiency of the DSSC with MoS_2-16 nm is approximately 25% higher than that of the DSSC with MoS_2-3 nm. The enhanced photovoltaic performances of the DSSC with the thicker MoS_2 film is resulted from the superior electrocatalytic activity, as confirmed by the CV and Tafel plots, and impedance data. As shown in Fig. S1 (Supplementary Material), the conversion efficiency of the DSSC with MoS_2-16 nm is only 7.8% lower than that of the DSSC with the conventional Pt CE (7.46%), indicating that the MoS_2 film prepared by ALD is a promising Pt-free electrocatalyst for solar cells.

Fig. 5b shows the incident photon-to-current conversion efficiency (IPCE) spectra of the fabricated DSSCs under front-illumination. Regardless of the MoS_2 layer thickness, all DSSCs exhibit similar IPCE spectra, which are related to the spectral responses of the N-719 dye molecules. The integrated photocurrents for DSSCs containing MoS_2 CEs with 3, 6, 9, 13, and 16 nm of MoS_2 layers are 11.05, 10.97, 12.13, 11.90, and 12.62 mA/cm^2, respectively. These results agree well with the J–V data.

To examine the photovoltaic performances of the bifacial DSSCs, the J–V characteristics and IPCE spectra were achieved under back-illumination, as shown in Fig. 6. The photovoltaic performance parameters determined under back-illumination are listed in Table 2. In general, the conversion efficiencies of the DSSCs under back-illumination are considerably lower than those under

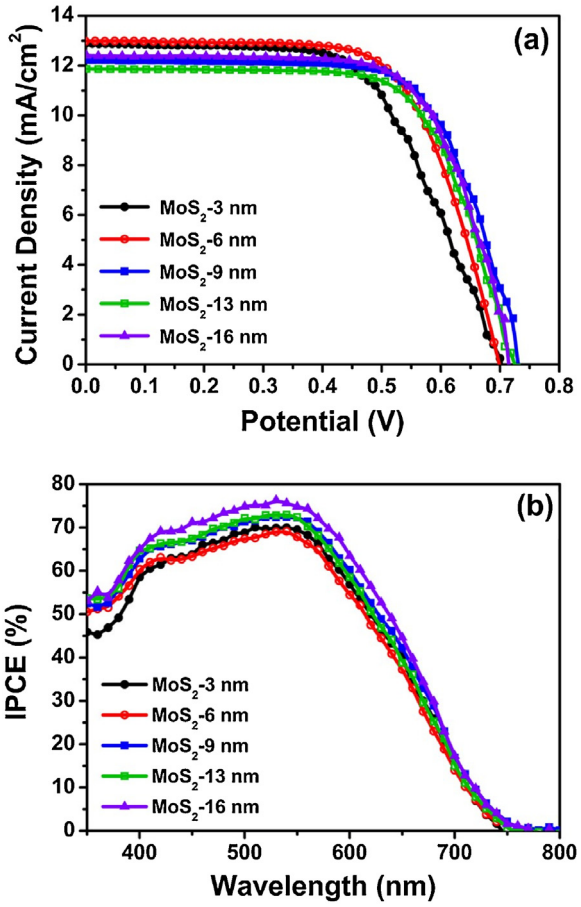

Fig. 5. (a) *J–V* characteristics and (b) IPCE spectra of DSSCs with MoS_2 CEs under front-illumination, as a function of MoS_2 film thickness.

Table 1
Variation in photovoltaic performance parameters of DSSCs with MoS_2 CEs under front-illumination, as a function of MoS_2 film thickness.

Thickness	J_{SC} (mA/cm^2)	V_{OC} (mV)	*FF*	η (%)
3 nm	12.88	702	0.61	5.52
6 nm	12.99	699	0.67	6.08
9 nm	12.93	730	0.68	6.42
13 nm	13.46	720	0.68	6.59
16 nm	13.96	714	0.69	6.88

front-illumination, because of the higher incident light loss for the CE and iodine electrolyte. The trends in the photovoltaic performance parameters of DSSCs under back-illumination is significantly different from those under front-illumination. The conversion efficiency gradually decreases as the thickness of the MoS_2 layer increases, because of the MoS_2 CE transmittance reduction, as confirmed by UV–Vis spectroscopy. Among the fabricated DSSCs, that with MoS_2-3 nm exhibits the highest J_{SC} and V_{OC}, and the lowest FF (Table 2), which are attributed to the superior transmittance and inferior electrocatalytic activity, respectively. Because the effect of transmittance is more dominant than that of the electrocatalytic activity, the DSSC with the MoS_2-3 nm film shows the highest conversion efficiency (4.28%) under back-illumination. The shapes of the IPCE spectra obtained under front-illumination (Fig. 5b) and back-illumination (Fig. 6b) are different; this difference is attributed to the difference in the incident light absorption, particularly in the short-wavelength region. The IPCE spectroscopy results agree well with the J–V data.

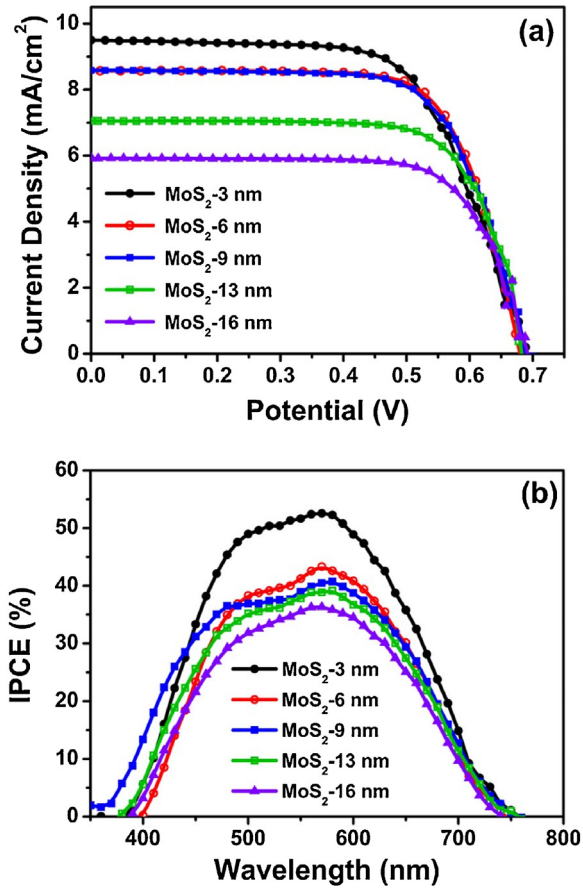

Fig. 6. (a) *J–V* characteristics and (b) IPCE spectra of DSSCs with MoS_2 CEs under back-illumination, as a function of MoS_2 film thickness.

Table 2
Variation in photovoltaic performance parameters of DSSCs with MoS_2 CEs under back-illumination, as a function of MoS_2 film thickness.

Thickness	J_{SC} (mA/cm^2)	V_{OC} (mV)	*FF*	η (%)
3 nm	9.50	693	0.65	4.28
6 nm	8.57	680	0.72	4.20
9 nm	8.67	693	0.69	4.15
13 nm	8.00	673	0.74	3.98
16 nm	6.67	689	0.72	3.31

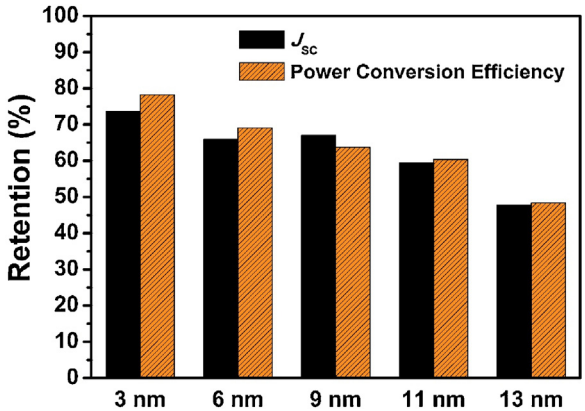

Fig. 7. J_{SC} and conversion efficiency retention rates (ratios of photovoltaic parameters obtained under back- and front-illumination), as a function of MoS_2 layer thickness.

The bifacial DSSC performances were compared by calculating the J_{SC} and conversion efficiency retention rates (ratios of photovoltaic parameters determined under back- and front-illumination), as a function of the MoS_2 layer thickness (Fig. 7). With increase in the MoS_2 layer thickness, the J_{SC} and conversion efficiency retention rates decrease. In addition, the J_{SC} and conversion efficiency retention values for the DSSCs are similar, indicating that conversion efficiency reduction under back-illumination is mainly due to the incident light loss and the resulting decrease in photocurrent. Although the electrocatalytic activity of MoS_2-3 nm is the lowest, it exhibits the highest conversion efficiency retention (78%).

Conclusions

In this study, transparent MoS_2 nanofilms with precisely controlled thickness of 3–16 nm are prepared by ALD. With increase in the MoS_2 layer thickness, although the surface area for electrochemical reaction remains constant, the electrocatalytic activity gradually increases, as revealed by the CV and Tafel plots, and impedance spectra. Under front-illumination, the DSSC conversion efficiency increases with an increase in the MoS_2 nanofilm thickness, because of electrocatalytic activity enhancement. In contrast, under back-illumination, the DSSC conversion efficiency decreases with increase in the MoS_2 nanofilm thickness because of optical transmittance reduction. Accordingly, under front-illumination, the 16 nm-thick-MoS_2 CE exhibits the highest conversion efficiency (6.88%), while under back-illumination, the 3 nm-thick MoS_2 CE exhibits the highest conversion efficiency (4.28%). It is noteworthy that only the 3 nm-thick MoS_2 film shows reasonable performances under both front- and back-illumination. We believe that these results will lead to significant advances in low-cost bifacial DSSCs for practical applications.

Acknowledgements

This work was supported by Basic Science Research Program (2017R1D1A1B03035077 and 2018R1D1A1B07047768) through the National Research Foundation of Korea (NRF) funded by the Ministry of Education, Republic of Korea. This work is also supported by Research Program (2018R1A2B2006708) and Technology Development Program to Solve Climate Changes (2015M1A2A2056824) funded by the National Research Foundation under the Ministry of Science and ICT, Republic of Korea. This work is also supported by the Korea Institute of Energy Technology Evaluation and Planning (KETEP) and the Ministry of Trade, Industry & Energy (MOTIE) of the Republic of Korea (2018201010636A).

Appendix A. Supplementary data

Supplementary material related to this article can be found, in the online version, at doi:https://doi.org/10.1016/j.jiec.2019.07.037.

References

[1] Z. Zheng, Q. Hu, S. Zhang, D. Zhang, J. Wang, S. Xie, R. Wang, Y. Qin, W. Li, L. Hong, N. Liang, F. Liu, Y. Zhang, Z. Wei, Z. Tang, T. Russell, J. Hou, H. Zhou, Adv. Mater. 30 (2018) 1801801.
[2] T. Kim, J. Heo, J.-Y. Lee, Y.-J. Yoon, T.H. Lee, Y.-S. Shin, I.-S. Kim, H. Kim, M.-S. Jeong, I.-W. Hwang, B. Walker, P.-S. Jo, B. Lim, J.-Y. Kim, ACS Appl. Mater. Interfaces 11 (2019) 7216.
[3] B. O'Regan, M. Grätzel, Nature 353 (1991) 737.
[4] A. Hagfeldt, G. Boschloo, L. Sun, L. Kloo, H. Pettersson, Chem. Rev. 110 (2010) 6595.
[5] K. Kakiage, Y. Aoyama, T. Yano, K. Oya, J.-i. Fujisawa, M. Hanaya, Chem. Commun. 51 (2015) 15894.
[6] K. Yoo, J.-Y. Kim, J.-A. Lee, J.-S. Kim, D.-K. Lee, K. Kim, J.-Y. Kim, B. Kim, H. Kim, W.-M. Kim, J.-H. Kim, M.-J. Ko, ACS Nano 9 (2015) 3760.
[7] J.-Y. Kim, J.-S. Kang, J. Shin, J. Kim, S.-J. Han, J. Park, Y.-S. Min, M.-J. Ko, Y.-E. Sung, Nanoscale 7 (2015) 8368.
[8] S. Ito, S.M. Zakeeruddin, P. Comte, P. Liska, D. Kuang, M. Grätzel, Nat. Photonics 2 (2008) 693.
[9] S.A. McDonald, G. Konstantatos, S. Zhang, P.W. Cyr, E.J. Klem, L. Levina, E.H. Sargent, Nat. Mater. 4 (2005) 138.
[10] J.-Y. Kim, J. Yang, J.-H. Yu, W. Baek, C.-H. Lee, H.-J. Son, T. Hyeon, M.-J. Ko, ACS Nano 9 (2015) 11286.
[11] J.-Y. Kim, Y.-J. Jang, J. Park, J. Kim, J.-S. Kang, D.-Y. Chung, Y.-E. Sung, C. Lee, J.-S. Lee, M.-J. Ko, Appl. Catal. B Environ. 227 (2018) 409.
[12] M.M. Lee, J. Teuscher, T. Miyasaka, T.N. Murakami, H.J. Snaith, Science 338 (2012) 643.
[13] M. Graetzel, R.A.J. Janssen, D.B. Mitzi, E.H. Sargent, Nature 488 (2012) 304.
[14] H.-S. Kim, C.-R. Lee, J.-H. Im, K.-B. Lee, T. Moehl, A. Marchioro, S.-J. Moon, R. Humphry-Baker, J.-H. Yum, J.E. Moser, M. Grätzel, N.-G. Park, Sci. Rep. 2 (2012) 591.
[15] J.-S. Kang, J.-Y. Kim, J. Yoon, J. Kim, J. Yang, D.-Y. Chung, M.-C. Kim, H. Jeong, Y.-J. Son, B.-G. Kim, J. Jeong, T. Hyeon, M. Choi, M.-J. Ko, Y.-E. Sung, Adv. Energy Mater. 8 (2018) 1703114.
[16] J.-H. Yum, T.W. Holcombe, Y. Kim, K. Rakstys, T. Moehl, J. Teuscher, J.H. Delcamp, M.K. Nazeeruddin, M. Grätzel, Sci. Rep. 3 (2013) 2446.
[17] M. Freitag, J. Teuscher, Y. Saygili, X. Zhang, F. Giordano, P. Liska, J. Hua, S.M. Zakeeruddin, J.-E. Moser, M. Grätzel, A. Hagfeldt, Nat. Photonics 11 (2017) 372.
[18] J.-S. Kang, J. Kim, J.-Y. Kim, M.-J. Lee, J. Kang, Y.-J. Son, J. Jeong, S.-H. Park, M.-J. Ko, Y.-E. Sung, ACS Appl. Mater. Interfaces 10 (2018) 8611.
[19] Y. Duan, Q. Tang, J. Liu, B. He, L. Yu, Angew. Chem. Int. Ed. 53 (2014) 14569.
[20] J. Miranda-Muñoz, S. Carretero-Palacios, A. Jime'nez-Solano, Y. Li, G. Lozano, H. Míguez, J. Mater. Chem. A 4 (2016) 1953.
[21] A. Khan, Y.-T. Huang, T. Miyasaka, M. Ikegami, S.-P. Feng, W.-D. Li, ACS Appl. Mater. Interfaces 9 (2017) 8083.
[22] J.-S. Kang, M.-A. Park, J.-Y. Kim, S.-H. Park, D.-Y. Chung, S.-H. Yu, J. Kim, J. Park, J.-W. Choi, K.-J. Lee, M.-J. Ko, K.-S. Ahn, Y.-E. Sung, Sci. Rep. 5 (2015) 10450.
[23] M. Wu, X. Lin, Y. Wang, L. Wang, W. Guo, D. Qi, X. Peng, A. Hagfeldt, M. Grätzel, T. Ma, J. Am. Chem. Soc. 134 (2012) 3419.
[24] Y.-C. Wang, D.-Y. Wang, Y.-T. Jiang, H.-A. Chen, C.-C. Chen, K.-C. Ho, H.-L. Chou, C.-W. Chen, Angew. Chem. Int. Ed. 52 (2013) 6694.
[25] Z. Li, F. Gong, G. Zhou, Z.-S. Wang, J. Phys. Chem. C 117 (2013) 6561.
[26] H. Jeong, J.-Y. Kim, B. Koo, H.-J. Son, D. Kim, M.-J. Ko, J. Power Sources 330 (2016) 104.
[27] D. Vikraman, S.-A. Patil, S. Hussain, N. Mengal, H.-S. Kim, S.-H. Jeong, J. Jung, H.-S. Kim, H.-J. Park, Dyes Pigm. 151 (2018) 7.
[28] S. Vijaya, G. Landi, J.J. Wu, S. Anandan, Electrochim. Acta 294 (2019) 134.
[29] Q.W. Jiang, G.R. Li, X.P. Pao, Chem. Commun. (2009) 6720.
[30] M. Wu, X. Lin, A. Hagfeldt, T. Ma, Angew. Chem. Int. Ed. 50 (2011) 3520.
[31] W.-J. Lee, E. Ramasamy, D.-Y. Lee, J.-S. Song, ACS Appl. Mater. Interfaces 1 (2009) 1145.
[32] T. Liu, X. Mai, H. Chen, J. Ren, Z. Liu, Y. Li, L. Gao, N. Wang, J. Zhang, H. He, Z. Guo, Nanoscale 10 (2018) 4194.
[33] L. Kavan, J.-H. Yum, K.N. Nazeeruddin, M. Grätzel, ACS Nano 5 (2011) 9171.
[34] J.-Y. Kim, J.-Y. Lee, K.-Y. Shin, H. Jeong, H.-J. Son, C.-H. Lee, J.-H. Park, S.-S. Lee, J.-G. Son, M.-J. Ko, Appl. Catal. B Environ. 192 (2016) 342.
[35] H.N. Tsao, J. Burschka, C. Yi, F. Kessler, M.K. Nazeeruddin, M. Grätzel, Energy Environ. Sci. 4 (2011) 4921.
[36] M. Wu, Y. Wang, X. Lin, N. Yu, L. Wang, L. Wang, A. Hagfeldt, T. Ma, Phys. Chem. Chem. Phys. 13 (2011) 19298.
[37] S.A. Patil, P.Y. Kalode, R.S. Mane, D.V. Shinde, A. Doyoung, C. Keumnam, M.M. Sung, S.B. Ambade, S.-H. Han, Dalton Trans. 43 (2014) 5256.
[38] B. Lei, G.R. Li, X.P. Gao, J. Mater. Chem. A 2 (2014) 3919.
[39] F. Li, J. Li, X. Lin, X. Li, Y. Fang, L. Jiao, X. An, Y. Fu, J. Jin, R. Li, J. Power Sources 300 (2015) 301.
[40] N. Liu, L. Yang, S. Wang, Z. Zhong, S. He, X. Yang, Q. Gao, Y. Tang, J. Power Sources 275 (2015) 588.
[41] H.-J. Chuang, B. Chamlagain, M. Koehler, M.M. Perera, J. Yan, D. Mandrus, D. Tománek, Z. Zhou, Nano Lett. 16 (2016) 1896.
[42] L. Yu, Y.-H. Lee, X. Ling, E.J.G. Santos, Y.C. Shin, Y. Lin, M. Dubey, E. Kaxiras, J. Kong, H. Wang, T. Palacios, Nano Lett. 14 (2014) 3055.
[43] X. Cao, Y. Shi, W. Shi, X. Rui, Q. Yan, J. Kong, H. Zhang, Small 9 (2013) 3433.
[44] S.-K. Park, S.-H. Yu, S. Woo, B. Quan, D.-C. Lee, M.-K. Kim, Y.-E. Sung, Y. Piao, Dalton Trans. 42 (2013) 2399.
[45] S. Shin, Z. Jin, D.H. Kwon, R. Bose, Y.-S. Min, Langmuir 31 (2015) 1196.
[46] M. Mattinen, T. Hatanpää, T. Sarnet, K. Mizohata, K. Meinander, P.J. King, L. Khriachtchev, J. Räisänen, M. Ritala, M. Leskelä, Adv. Mater. Interfaces 4 (2017) 1700123.
[47] Z. Jin, S. Shin, D.H. Kwon, S.-J. Han, Y.-S. Min, Nanoscale 6 (2014) 14453.
[48] J. Tian, Q. Zhang, E. Uchaker, R. Gao, X. Qu, S. Zhang, G. Cao, Energy Environ. Sci. 6 (2013) 3542.
[49] J.-Y. Kim, K.-H. Lee, J. Shin, S.-H. Park, J.-S. Kang, K.-S. Han, M.-M. Sung, N. Pinna, Y.-E. Sung, Nanotechnology 25 (2014) 504003.
[50] J.D. Roy-Mayhew, D.J. Bozym, C. Punckt, I.A. Aksay, ACS Nano 4 (2010) 6203.
[51] J.-Y. Kim, K.-J. Lee, S.-H. Kang, J. Shin, Y.-E. Sung, J. Phys. Chem. C 115 (2011) 19979.
[52] L. Han, N. Koide, Y. Chiba, T. Mitate, Appl. Phys. Lett. 84 (2004) 2433.
[53] J.-Y. Kim, K.-Y. Shin, M.H. Raza, N. Pinna, Y.-E. Sung, Korean J. Chem. Eng. 36 (2019) 1157.